LA-UR-15-28086
Approved for public release; distribution is unlimited.

Title: Report on simulation of fission gas and fission product diffusion in UO2

Author(s): Andersson, Anders David Ragnar
Perriot, Romain Thibault
Pastore, Giovanni
Tonks, Michael
Cooper, Michael William Donald
Liu, Xiang-Yang
Goyal, Anuj
Uberuaga, Blas P.
Stanek, Christopher Richard

Intended for: Report

Issued: 2016-07-22 (rev.1)

# Report on simulation of fission gas and fission product diffusion in $UO_2$

David Andersson[1], Romain Perriot[1], Giovanni Pastore[2], Michael R. Tonks[2], Michael Cooper[1], Xiang-Yang Liu[1], Anuj Goyal[3], Blas P. Uberuaga[1] and Christopher R. Stanek[1]

[1]Materials Science and Technology Division, Los Alamos National Laboratory Los Alamos, NM 87545

[2]Fuel Modeling and Simulation Department, Idaho National Laboratory, P.O. Box 1625, Idaho Falls, ID 83415

[3]Department of Materials Science and Engineering, University of Florida, Gainesville, Florida 32611, USA

Report on Milestone:
M2MS-15LA0201031: Issue Final Report on simulations of fission gas and fission product diffusion in $UO_2$

# Abstract

In $UO_2$ nuclear fuel, the retention and release of fission gas atoms such as xenon (Xe) are important for nuclear fuel performance by, for example, reducing the fuel thermal conductivity, causing fuel swelling that leads to mechanical interaction with the clad, increasing the plenum pressure and reducing the fuel–clad gap thermal conductivity. We use multi-scale simulations to determine fission gas diffusion mechanisms as well as the corresponding rates in $UO_2$ under both intrinsic and irradiation conditions. In addition to Xe and Kr, the fission products Zr, Ru, Ce, Y, La, Sr and Ba have been investigated. Density functional theory (DFT) calculations are used to study formation, binding and migration energies of small clusters of Xe atoms and vacancies. Empirical potential calculations enable us to determine the corresponding entropies and attempt frequencies for migration as well as investigate the properties of large clusters or small fission gas bubbles. A continuum reaction-diffusion model is developed for Xe and point defects based on the mechanisms and rates obtained from atomistic simulations. Effective fission gas diffusivities are then obtained by solving this set of equations for different chemical and irradiation conditions using the MARMOT phase field code. The predictions are compared to available experimental data. The importance of the large $Xe_{U3O}$ cluster (a Xe atom in a uranium + oxygen vacancy trap site with two bound uranium vacancies) is emphasized, which is a consequence of its high mobility and high binding energy. We find that the $Xe_{U3O}$ cluster gives Xe diffusion coefficients that are higher for intrinsic conditions than under irradiation over a wide range of temperatures. Under irradiation the fast-moving $Xe_{U3O}$ cluster recombines quickly with irradiation induced interstitial U ions, while this mechanism is less important for intrinsic conditions. The net result is higher concentration of the $Xe_{U3O}$ cluster for intrinsic conditions than under irradiation. We speculate that differences in the irradiation conditions and their impact on the $Xe_{U3O}$ cluster can explain the wide range of diffusivities reported in experimental studies. However, all vacancy-mediated mechanisms underestimate the Xe diffusivity compared to the empirical radiation-enhanced rate used in most fission gas release models. We investigate the possibility that diffusion of small fission gas bubbles or extended Xe-vacancy clusters may give rise to the observed radiation-enhanced diffusion coefficient. These studies highlight the importance of U divacancies and an octahedron coordination of uranium vacancies encompassing a Xe fission gas atom. The latter cluster can migrate via a multistep mechanism with a rather low effective barrier, which together with irradiation-induced clusters of uranium vacancies, gives rise to the irradiation-enhanced diffusion coefficient observed in experiments.

# 1. Introduction and background

During several years we have studied fission gas (Xe and Kr) [1-7] and fission product (Zr, Ru, Ce, Y, La, Sr and Ba) [8] diffusion in $UO_2$ and $UO_{2\pm x}$, both under intrinsic conditions and under irradiation, using density functional theory calculations, empirical potential calculations and MARMOT simulations. The results have been presented in several papers [1-8], starting with investigating the preferred Xe trap site, how Xe atoms may migrate by binding vacancies or occupying interstitial sites, estimating the vacancy concentration enabling Xe diffusion and finally putting all the pieces together in MARMOT and also extending the results for Xe to Kr and the other fission products referenced above.

The active diffusion mechanism for Xe emerging from these studies involves Xe occupying uranium vacancy trap sites (possibly with additional oxygen vacancies) and another bound uranium vacancy enabling diffusion (see Figure 1). Under irradiation the diffusion coefficient increases at intermediate to low temperatures, which is thought to be a consequence of increasing the concentration of uranium vacancies and thus the fraction of mobile Xe clusters. This is consistent with the often-used empirical model derived by Turnbull [9-12]. Figure 2 shows the Xe diffusivity in stoichiometric $UO_2$ obtained from DFT/empirical potential/MARMOT simulations and compares the results to available experimental data and empirical model predictions [2,3,11,13,14]. MARMOT uses the DFT/empirical potential values controlling the diffusion rate of each mechanism and averages the contribution from all of them based on the thermodynamic and irradiation conditions to give an effective diffusivity. Figure 3 compares the calculated diffusivity of Xe to other fission products under intrinsic conditions [8]. With exceptions for Ru, the fission products diffuse much slower than Xe, which is consistent with the accepted understanding even though there is very little experimental data for validation.

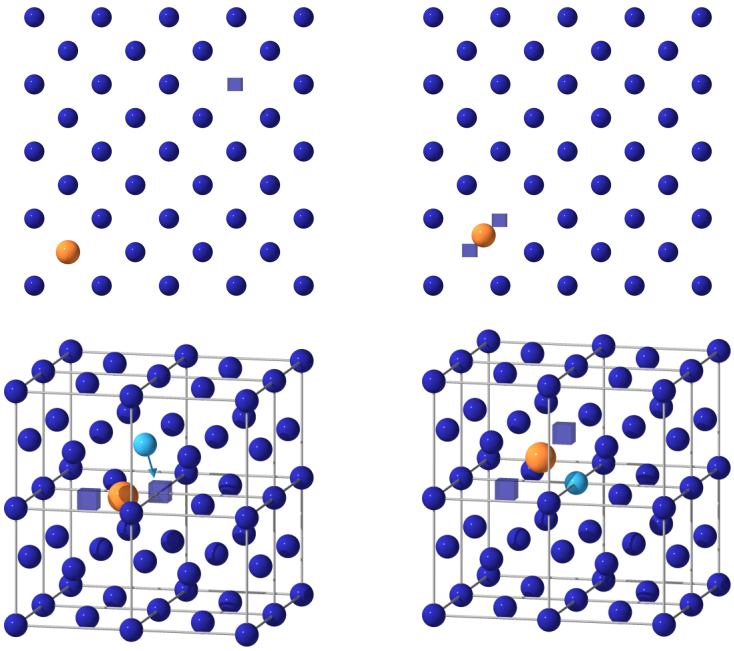

**Figure 1: Schematic illustration of Xe diffusion in $UO_2$ by a vacancy mechanism. To simplify visualization, the oxygen sublattice has been omitted. Xe atoms are shown as yellow spheres, blue spheres represent uranium ions and blue squares uranium vacancies. Here Xe occupies a uranium vacancy trap site and diffusion is mediated by another uranium vacancy. The diffusion coefficient is determined by the probability of having a vacancy next to the Xe trap site, which is governed by the vacancy formation energy and the binding energy, and the barrier for intra-cluster uranium vacancy migration. Migration of the Xe atom from one side of the cluster to the other occurs with a very low barrier and thus does not enter the expression for the diffusion coefficient. This is the simplest vacancy diffusion mechanism. As explained in this report, there are several other mechanisms involving more complicated trap sites and vacancy clusters, however the basic steps are still the same (binding of vacancies mediating diffusion and one or several migration steps of the cluster components leading to net transport of the Xe atom). The Zr, Ru, Ce, Y, La, Sr and Ba fission products diffuse by the same type of mechanism.**

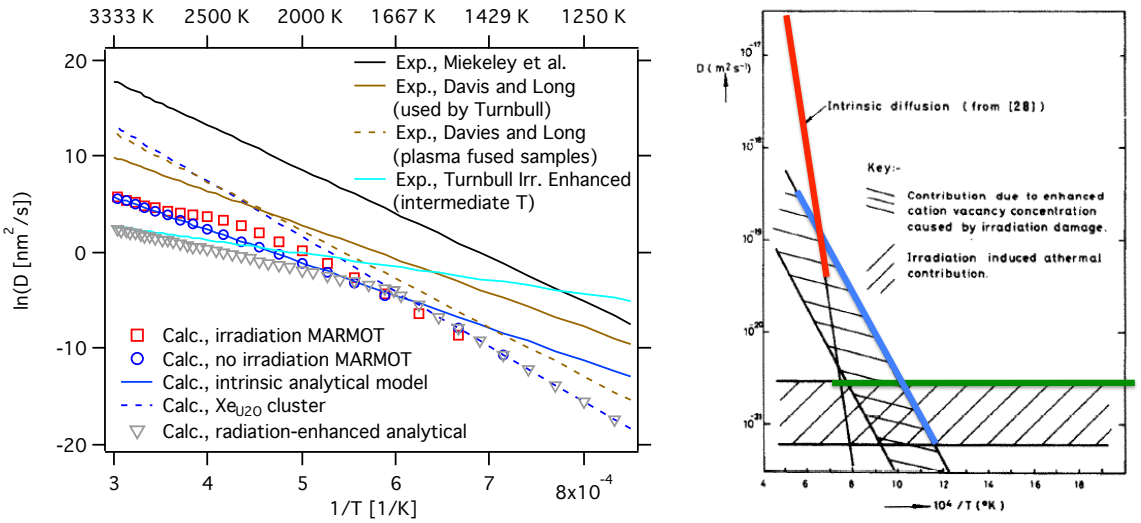


**Figure 2: Left) The Xe diffusivity under irradiation conditions compared to the intrinsic diffusivity (Calc., MARMOT), the corresponding analytical expressions derived in Ref. [2] and experimental data [13,14]. Note the underestimation compared to experimental data. Right) The fission gas diffusion model proposed by Turnbull et al. [11] and used in most existing fission gas release models. The colors highlight the intrinsic (red, $D_1$), radiation-enhanced (blue, $D_2$) and radiation-induced (green, $D_3$) diffusion regimes.**

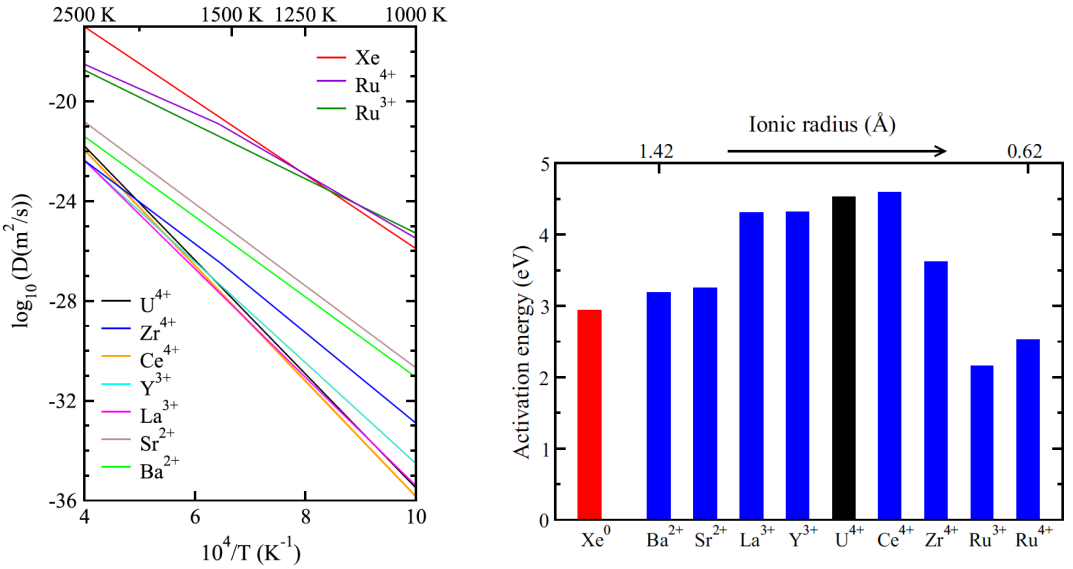


**Figure 3: Left) Diffusion coefficient for solid fission products, U self-diffusion, and Xe in $UO_2$. For each solid fission products, only the active mechanism (i.e. limiting rate) is shown. Right) Comparison of the corresponding activation energies as function of the ionic radii of the fission products. These two figures are reproduced from [8].**

Most fission gas release models rely on the analysis by Turnbull et al. for description of the diffusion of Xe atoms in bulk $UO_2$ (Stage 1 of fission gas release) [9-11,15,16]. The diffusivity or diffusion coefficient in these models refers to Xe, which is the most important fission gas atom. Turnbull et al. divided the diffusivity into three temperature ranges [9-11,15]. At high temperature ($D_1$, T > 1650 K) intrinsic diffusion dominates and the diffusivity for stoichiometric $UO_2$ was taken from Davies and Long [13], who reported an activation energy of 3.04 eV ($E_a$) and a pre-exponential factor ($D_0$) of 7.6 $\times 10^{-10}$ $m^2/s$,

$$D = D_0 \exp\left(-\frac{E_a}{k_B T}\right).$$

The uncertainty in the fission gas diffusion coefficient has been discussed in many papers and continuous to be a challenge from both experimental and modeling perspectives. For example, at 1400°C diffusivities have been found to range many orders of magnitude between studies [17], which can be attributed to several experimental factors of which sample non-stoichiometry (x in $UO_{2\pm x}$) was identified as the most important [17]. The sample non-stoichiometry is controlled by temperature and the chemistry of the experimental setup, for example, whether the measurement was carried out in vacuum or in flowing $H_2$ gas, and the material used for the sample holder. Experimental data for the activation energies span values from 2.87 eV to 3.95 eV and pre-exponential factors from $5 \times 10^{-4}$ $m^2/s$ to $2.90 \times 10^{-12}$ $m^2/s$ [14,18,19]. Typically, a higher activation energy is compensated by a higher pre-exponential factor, which is expected since the stoichiometry is maintained close to $UO_2$ for all cases. The results due to Davies and Long [13] and Miekeley et al. [14] are plotted in Figure 2. We report two data sets from Davies and Long [13], the

first corresponds to the model used in the fission gas release simulations and the second to measurements on plasma fused samples annealed in vacuum at 1650°C (in addition to the sintering procedure used for the first sample set). Clearly, the two samples give different answers, however the explanation for this behavior has not been identified.

In the intermediate temperature range ($D_2$, 1381 < T < 1650 K), radiation-enhanced diffusion dominates over intrinsic diffusion, i.e. more defects are generated by irradiation than by thermal processes. The activation energy was derived from a rate theory model of the concentration of radiation-induced vacancies (proportional to the square root of the fission rate, $\dot{F}$) and the assumption that the rate-limiting step for Xe transport is diffusion of uranium vacancies [11,12], which gives an activation energy of 1.20 eV and $D_0 = 4 \cdot 1.41 \cdot 10^{-25} \cdot \sqrt{\dot{F}}$ m$^2$/s. Below 1381 K ($D_3$), Xe diffusion is athermal and proportional to the fission rate [11,12,20]. The Turnbull model for irradiation-enhanced diffusion is also plotted in Figure 2.

Although analysis of diffusion data allows for determination of $D_1$, $D_2$ and $D_3$, there is still uncertainty regarding diffusion mechanisms as well as the detailed relation between diffusivities and the thermodynamic (i.e. non-stoichiometry) and irradiation conditions. This is important to understand in order to enable modeling of new operating conditions, new fuel types (composition and microstructure) and accident scenarios as well as improving the accuracy of current models. Comparing our predicted diffusivities to the experimental data highlights this lack of understanding. As can seen in Figure 2, the calculated diffusivities are underestimated compared to experiments. Even though the experiments are difficult to perform and the variation between different sources fairly significant [17], the calculations are consistently too low. This conclusion is valid for both intrinsic conditions and under irradiation (the damage rate, which is governed by the fission rate $\dot{F}$, was assumed to be $4.05 \times 10^{-6}$ defects/U atom s following Turnbull [10], see Ref. [2] for additional details). At low temperatures, the Xe diffusion coefficient is limited by the mobility of the Xe-vacancy clusters. A majority of the Xe atoms occupy mobile Xe-vacancy clusters due to the strong binding energy between trap sites and uranium vacancies. Changing, for example, the irradiation conditions to create more vacancies do not result in increased Xe diffusion coefficient according to this mechanism. In particular, this leads to significant underestimation of the Xe diffusivity for the radiation-enhanced regime at low temperatures, but the diffusivity is also predicted to be too low for the intrinsic regime at higher temperatures. Obviously, the lower diffusion coefficients directly translate to lower fission gas release. This is illustrated in Figure 4 (red curve), showing BISON simulations of fission gas release for two different test cases [3,21,22]. The BISON results were obtained with the standard model using the Xe diffusivity derived by Turnbull from experiments and our new theoretical model, including both the $Xe_{U2O}$ and $Xe_{U3O}$ (explained later) clusters.

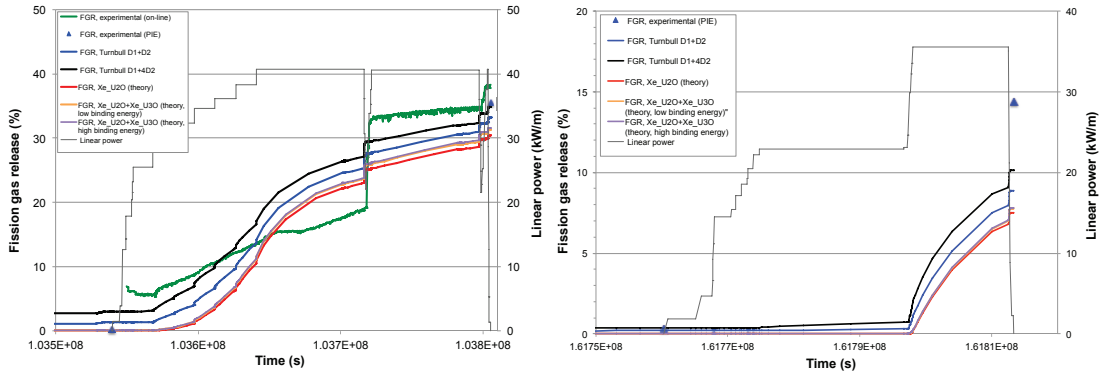


**Figure 4: Left) BISON simulation of fission gas release for the Risø-3 AN3 experiment [21] using a number of different fission gas diffusion models. Right) The same plot as in a), but for the Risø GE7 experiment [22]. All theoretical models predict lower release than existing empirical models and measurements, which is consistent with the lower values for the Xe diffusivity in Figure 2.**

The upper bound imposed by the Xe-vacancy cluster mobilities implies that the reason for underestimating the Xe diffusion coefficients compared to experiments is likely related to neglecting diffusion of extended (large) Xe-vacancy clusters in the model used in Refs. [1,2]. Highly mobile Xe interstitials could be another option [4], however our MARMOT simulations incorporating this mechanism show that the interstitials recombine with uranium vacancies too quickly to provide any significant contribution to the total Xe diffusivity. Extended clusters refer to those involving more than one uranium vacancy (in addition to the trap site vacancy). The clusters may also include one or several oxygen vacancies. We have studied the contribution from such clusters by calculating the stability as function of size and the detailed atomic configuration, the barriers for moving vacancies or atoms within and around the cluster and the binding energy of uranium vacancies or divacancies to the cluster. We have also investigated surface segregation and surface diffusion of vacancies, which is intended to represent the rate-limiting step and thermodynamics for diffusion of small fission gas bubbles known to exist in the fuel under irradiation. The diffusion concept involving small bubbles or large clusters is illustrated in Figure 5.

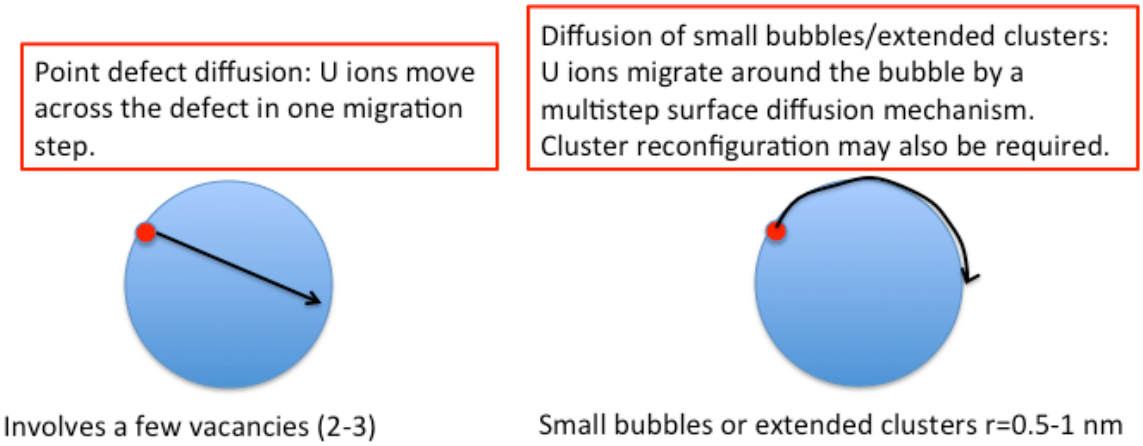


**Figure 5: Schematic illustration highlighting the difference between point defect diffusion of fission gas atoms and diffusion of extended clusters or small fission gas bubbles.**

This report summarizes the progress in modeling extended Xe defect clusters and uranium vacancies (single vacancies and divacancies), their mobility and how they may impact diffusion coefficients for both the intrinsic and irradiation-enhanced regime. These mechanisms are much more complicated than the small clusters that have so far assumed to be responsible for Xe diffusion. The complexity of these diffusion mechanisms imply that additional work remains to be performed before the model can be completed.

# 2. Methodology

The density functional theory (DFT) calculations were carried out with the VASP code using the LDA+*U* formalism for the uranium f electrons. These calculations were used to estimate defect energies and migration barriers, while empirical potential calculations applying the Basak $UO_2$ potential [23] were used for the corresponding entropies, due to the high computational cost to obtain them from DFT calculations. For further information about the DFT and empirical potential methodology we refer to Refs. [1,2].

In all existing studies the defective energies and migration barriers were calculated using 2×2×3 $UO_2$ supercells and charged defects were corrected for finite size effects and slow convergence with respect to the size of the supercell according to the established methodology [24]. However, for defects with high charge states, such as fully charged bound uranium vacancies (uranium divacancies with a maximum charge of -8), the accuracy of the corrections and thus the calculated defect energies are diminished. As part of an exercise to validate our modeling approach and assumptions we have started performing simulations using 3×3×3 supercells. The reason for applying the smaller supercells in earlier studies is simply the high computational cost associated with the larger supercells. Here, we report initial results and discuss conclusions from the calculations on 3×3×3 supercell. These larger supercells are also necessary in order to treat some of the extended Xe-vacancy clusters investigated in this study.

The MARMOT code [25] was used to solve a set of coupled differential equations describing defect formation, clustering and diffusion from which effective Xe diffusivities can be extracted [3]. Further information about the MARMOT simulations can be found in Ref. [3]. All MARMOT results presented here are based on DFT data obtained from the 2×2×3 supercells.

# 3. Results and discussion

This section first addresses diffusion of uranium vacancies and divacancies, followed by Xe diffusion by vacancy mechanisms and in particular the importance of extended Xe-vacancy clusters sharing features with uranium divacancies. The next step is to investigate diffusion of idealized small fission gas bubbles represented by (111) surfaces and whether they can explain the radiation-enhanced diffusion occurring in-pile at intermediate to low temperatures. Finally, we identify an octahedron configuration of six uranium and eight oxygen vacancies as being the

most likely candidate for enabling fast Xe diffusion and understanding radiation-enhanced diffusion of Xe and vacancies. This cluster can be viewed as the smallest nucleus of a fission gas bubble.

## 3.1 Diffusion of uranium vacancies and divacancies

Xe diffusion is closely related to diffusion of uranium vacancies, which enable Xe migration according to mechanisms following the principles shown in Figure 1. Consequently, as a first step to understanding Xe diffusion we have investigated uranium vacancy diffusion [1,2,26,27].

Table 1 summarizes the migration barriers and binding energies of uranium divacancy clusters obtained from DFT calculations using the 2×2×3 and 3×3×3 supercells. The migration barriers for single uranium vacancies are also included. The barrier for the divacancy cluster is reduced by about 2 eV compared to single vacancies. The charged defects have a lower barrier than the neutral defects, which is largely a consequence of the increased local volume for the former case. The $U^{5+}$ ions present around the neutral defects contract the lattice. The barriers are quite similar for the 2×2×3 and 3×3×3 supercells, while the binding energy for charged uranium divacancies exhibit significant variation between the 2×2×3 and 3×3×3 supercells. The binding energies for neutral clusters vary less. This is expected based on the long-range Coulomb interactions present in the charged systems. The simulations attempt to correct for the finite size of the supercells by applying extrapolation schemes outlined in [24] and used in all of our studies. However, for highly charged defects such as uranium divacancies the correction scheme partially fails, which is not a big surprise. The new 3×3×3 supercell calculations will eventually allow us to narrow down these uncertainties significantly, but additional calculations must first be performed (in progress) to complete the picture.

We have investigated the balance between single vacancies and divacancies by implementing a simple rate-theory model in MARMOT. From MARMOT simulations of the concentration of point defects under irradiation we have calculated the resulting uranium self-diffusivity to be $D=1.26\times10^{-18}\times\exp(-2.21\ \text{eV}/k_BT)\ \text{m}^2/\text{s}$. Above roughly 1400-1500 K thermal or intrinsic diffusion dominates over radiation-enhanced mechanisms. However, uranium divacancies are still the major contributor to diffusion in $UO_2$ giving $E_a= 4.17$ eV and $D_0 = 6.11\times10^{-11}\ \text{m}^2/\text{s}$ to be compared to the experimental values of $E_a=4.4$ eV and $D_0=5.84\times10^{-11}\ \text{m}^2/\text{s}$ for the same conditions. Uranium self-diffusion mediated by single vacancies occur at a slower rate than divacancies, corresponding to $E_a=5.44$ eV and $D_0=3.2\times10^{-10}\ \text{m}^2/\text{s}$. The results above refer to the thermodynamics and kinetics obtained from the 2×2×3 supercells. The higher formation energy and lower binding energy obtained from the 3×3×3 supercells should shift the activation energies to slightly higher values. The corresponding simulations and analysis will be completed in FY16.

The main conclusion from these studies is that uranium divacancies have a much lower migration barrier than single uranium vacancies. This follows from reduced

repulsion by neighboring uranium ions at the saddle point, because one of these ions is missing. Figure 6 illustrates the divacancy migration pathway and highlights its curved nature traversing an octahedral interstitial site. Moreover, the uranium ions prefer to be fully coordinated with oxygen ions, which imply that the migration barrier increases if the clusters also include oxygen vacancies, in particular if these are located in the vicinity of the saddle point. One way of, at least partially, reducing this penalty is to include a neighboring oxygen ion in the uranium ion migration process (see Table 1). The latter barrier is very close to the barrier for uranium divacancies. The binding energy of uranium divacancies depends on the charge state of the cluster. The interaction for neutral clusters is neither repulsive nor attractive (close to zero), while the fully charged clusters are repelled according to the 3×3×3 supercell calculations and slightly attractive according to the smaller 2×2×3 supercell. The 3×3×3 supercell should give the most reliable result. Even after accounting for the binding energies, due to the much lower migration barrier of uranium divacancies compared to single uranium vacancies, the former defect type dominates diffusion in $UO_2$ under irradiation and possibly even under intrinsic conditions.

**Table 1: Binding and migration energies of uranium divacancies ($V_{U2}$) in $UO_2$. The superscripts x (neutral) and "" (-8) denote the charge state of the defects. The migration barriers of single uranium vacancies ($V_U$) and the $V_{U2O}$ cluster are also shown.**

| Defect type | Migration barrier (eV) 2×2×3 | Binding energy (eV) 2×2×3 | Migration barrier (eV) 3×3×3 | Binding energy (eV) 3×3×3 |
|---|---|---|---|---|
| $V^{x}_{U}$ | 4.95 | -- | 5.45 | -- |
| $V''''_{U}$ | 4.72 | -- | -- | -- |
| $V^{x}_{U2}$ | 3.27 | -0.01 | 3.17 | 0.32 |
| $V''''''_{U2}$ | 2.84 | -0.30 | -- | 1.05 |
| $V^{x}_{U2O}$ | -- | -- | 3.31 | -- |

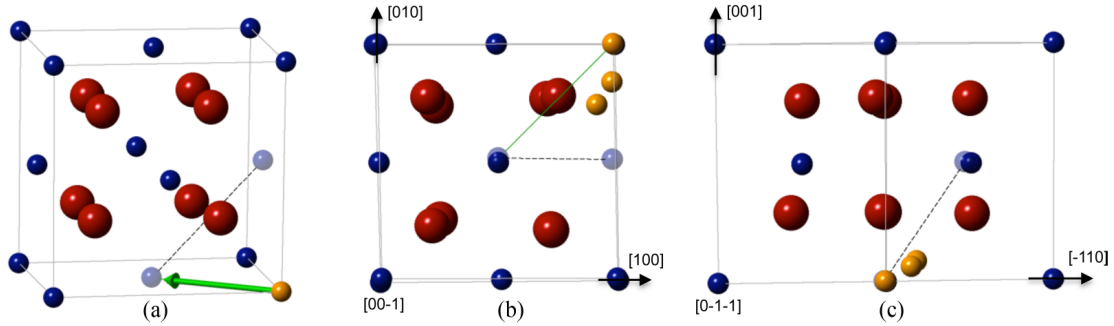


**Figure 6: (a) Schematic showing that the migration of a uranium divacancy (dashed line) is related to the migration of one of its constituent vacancies. (b) Combined snapshots of the migrating uranium ion [shown in yellow in (a)] to the nearest vacancy along <110> direction, as determined from the DFT calculations. The green solid line represents straight path along <110>, but from the snapshots it is clearthat the path is curved away from the <110> direction as well as tilted (c) from the (001) plane, similar to the behavior for the single vacancy as discussed in the text. This figure is reproduced from [26].**

## 3.2 Diffusion of Xe clusters involving one or two uranium vacancies

Identifying the contribution of divacancies to diffusion is also a key step towards accurately predicting Xe diffusion. As outlined in the introduction the simplest Xe-vacancy cluster involving one bound uranium vacancy to the Xe trap site (denoted $Xe_{U2O}$) cannot reproduce experimental diffusivities obtained from release experiments, simply because the migration barrier is too high. Based on the findings for uranium divacancies, we have investigated the properties of a cluster formed by binding two uranium vacancies to the Xe trap site (denoted $Xe_{U3O}$). The idea being that the migration barrier may be reduced similar to the mechanism observed for divacancies. Additionally, the large cluster may reduce the blocking effect of the Xe atom getting close the migrating uranium ion at the saddle point. Figure 7 illustrates the two migration steps involved in achieving long-range diffusion for the $Xe_{U3O}$. The migration barrier for this cluster is about 1 eV lower than for the smaller $Xe_{U2O}$ cluster and it is also strongly bound.

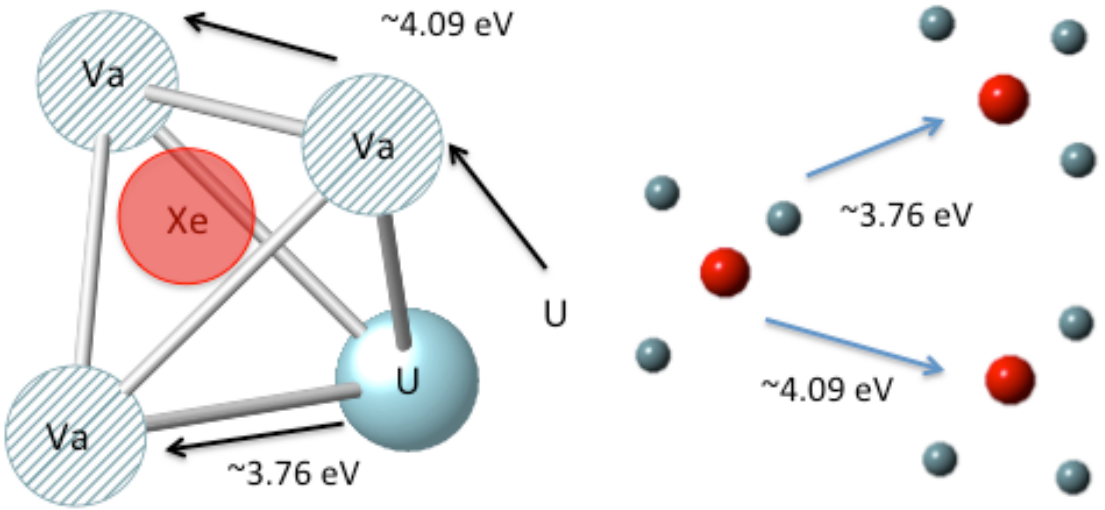


**Figure 7: The migration steps involved in diffusion of the $Xe_{U3O}$ cluster. The step starting with migration of the nearest neighbor uranium ion on the right hand side (4.09 eV) is necessary for long-range diffusion, because the other step (3.76 eV) only leads to the cluster changing orientation back and fourth. The right hand figures show the vacancies composing the $Xe_{U3O}$ cluster and how diffusion of the cluster occurs. Uranium or uranium vacancies are shown in grey and oxygen or oxygen vacancies in red.**

Even though the concentration of $Xe_{U3O}$ clusters is small, its high mobility compared to the $Xe_{U2O}$ cluster gives a significant contribution to the diffusivity across almost the full temperature range (see Figure 8). At the highest temperatures in our simulations the diffusivity approaches the result when only the $Xe_{U2O}$ cluster is included, which also corresponds to the intrinsic result for the $Xe_{U2O}$ model. Below the highest temperatures the diffusivity is controlled by cluster diffusion. There is a balance between the $Xe_{U2O}$ and $Xe_{U3O}$ clusters, which implies that the effective diffusivity lies between these two limiting cluster diffusivities. This behavior extrapolates to low temperature. In the transition between the very high temperature behavior and the lower or intermediate temperature regime there is a switch from the $Xe_{U2O}$ cluster limited by the vacancy concentration (very high temperature) to a combination of the $Xe_{U2O}$ and $Xe_{U3O}$ clusters at lower

temperatures. This gives rise to small temperature range with increasing diffusivity as temperature decreases. The diffusivity for the $Xe_{U3O}$ model in the intermediate temperature range agrees quite well with Turnbull's model [11,12], which is based on the diffusivity data from Davies and Long [13]. Note that the relevant range for this model is from just above 2000 K to about 1400-1500 K, where the agreement between the theoretical model and experiments is quite good. Davies and Long [Davies] found a range of diffusivities for different samples and our model agrees best with the results for plasma fused samples [13], in particular for the activation energy (slope of the diffusivity curves). The magnitude of the diffusivity is similar between the different samples investigated by Davies and Long [13]. However, while our simulations refer to in-pile conditions, the experiments by Davies and Long [13] were out-of-pile post-irradiation release experiments for which intrinsic conditions are typically assumed to be prevalent. Our results indicate that the effect of irradiation cannot always be ignored in the post-irradiation annealing experiments, which is further discussed in the next paragraph. At low temperature the diffusivity is still underestimated compared to the irradiation induced model proposed by Turnbull [11,12].

We have also performed simulations for the $Xe_{U3O}$ model without irradiation (see Figure 8). Surprisingly, the diffusivity increases rather than decreases with respect to the simulations with active defect production due to irradiation. This is contrary to our intuition and it is explained by the concentration of $Xe_{U3O}$ clusters increasing due to decreased recombination with uranium interstitial ($U_I$) defects. Under intrinsic conditions the interstitial concentration is very small, essentially negligible. At very high temperature the results again agree with the $Xe_{U2O}$ model, but in the intermediate range the diffusivity now exceeds that in Turnbull's model [11,12] based on the Davies and Long data [13]. Interestingly, the diffusivity agrees very well with the data reported by Miekeley et al. [14]. This correlates with the Miekeley et al. [14] samples being exposed to orders of magnitude smaller irradiation dose than the dose in the experiments by Davies and Long [13], which presumably correlates with the concentration of interstitials available for recombination with $Xe_{U3O}$ clusters in the diffusion anneal experiments, even though the quantitative relation remains to be worked out. This implies that the $Xe_{U3O}$ cluster contributes significantly to diffusion of Xe in nearly stoichiometric $UO_2$ due to a combination of its high stability and high mobility. The contribution from this cluster is higher for intrinsic conditions than under irradiation, which helps to explain some of the discrepancies between different experimental measurements, see Figure 8. In fact, the decrease in Xe diffusivity with increased irradiation has been observed in existing studies [28], but has traditionally been attributed to increased trapping. Additional work is required before we can draw solid conclusions regarding the relative importance of trapping and decreased concentration of mobile clusters due to interstitial recombination. Regardless, the $Xe_{U3O}$ model cannot explain the increased irradiation induced diffusivity proposed by Turnbull [11,12] in the intermediate to low temperature range.

There is some uncertainty for the binding energy of the $Xe_{U3O}$ cluster due to the challenges associated with DFT calculations of such a large cluster with high charge, which was emphasized for uranium divacancies by comparing results from the 2×2×3 and 3×3×3 supercells. We have not yet been able to investigate the $Xe_{U2O}$ or $Xe_{U3O}$ clusters with the larger supercells. However, we have performed MARMOT simulations with the vacancy binding energy set to -1.99 eV instead of -3.27 eV used in the simulations referenced above. The results are also shown in Figure 8 and, as expected, the diffusivity lies in between the high binding energy and the result excluding the $Xe_{U3O}$ cluster. Even with the reduced binding energy, the general conclusion regarding the increased diffusion rate of Xe due to the $Xe_{U3O}$ cluster remains valid.

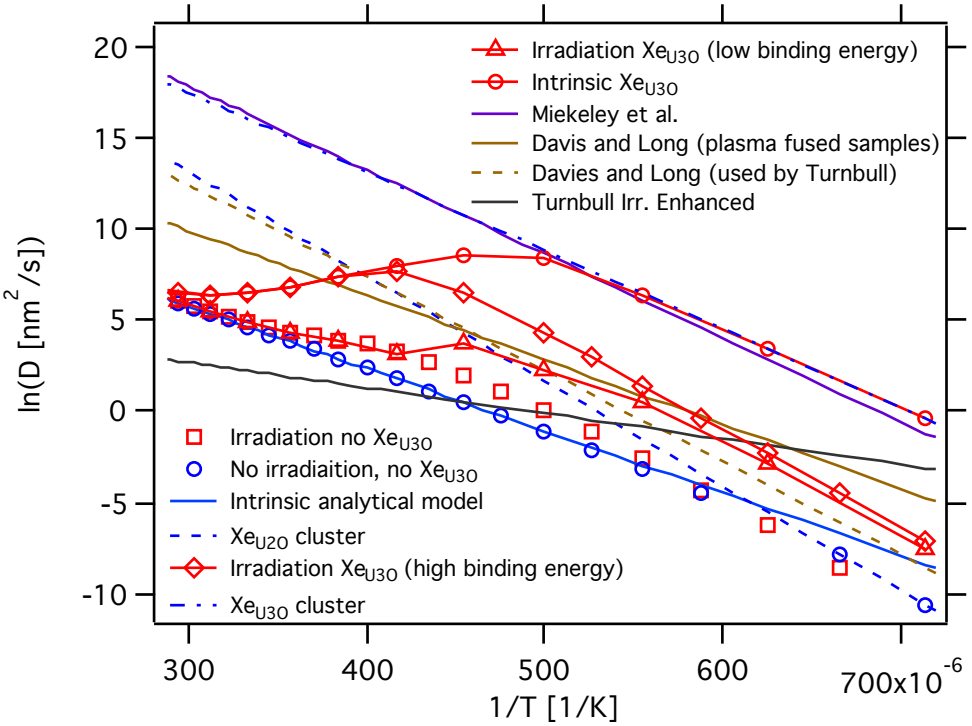


**Figure 8: The Xe diffusion coefficient for mechanisms involving both the $Xe_{U2O}$ and $Xe_{U3O}$ clusters. The $Xe_{U3O}$ cluster gives the highest diffusivity, which agrees well with experiments for the intrinsic regime, but still underestimates the diffusivity at low temperatures where radiation–enhanced diffusion dominates. The plot also illustrates the influence of the $Xe_{U3O}$ binding energy and that recombination between the $Xe_{U3O}$ cluster and U interstitials leads to decreasing diffusivity under irradiation.**

## 3.3 Diffusion of small fission gas bubbles or extended Xe-vacancy clusters

The various options for Xe diffusion under irradiation investigated in Figure 8 all fail to capture the intermediate and low temperature irradiation-enhanced diffusivity proposed by Turnbull [11,12] (this refers to the activated intermediate temperature diffusivity and not the athermal diffusion at the lowest temperatures). Based on the present results it is difficult to envision a simple vacancy or point defect mechanism that gives such a low activation energy and also very low pre-exponential factor. Diffusion of small fission gas bubbles is another mechanism that could be

responsible for the irradiation-enhanced diffusivity. Small bubbles are well known to be present in irradiated fuels as a consequence of the low solubility of Xe in the $UO_2$ matrix. However, this contribution is typically thought to be negligible in fission gas release models based on experimental measurements on irradiated fuel showing low mobility of bubbles [29,30]. Nevertheless, we investigate this possibility because simple point defect diffusion mechanisms ($Xe_{U2O}$ and $Xe_{U3O}$) fail to capture this behavior. It is also possible that the in-pile conditions differ sufficiently from the out-of-pile experiments used to conclude that bubble diffusion is very slow.

Bubble diffusion may be controlled by one of three mechanisms transferring atoms from one side of the bubble to the other: 1) volume diffusion of vacancies in the bulk around the bubble, 2) surface diffusion and 3) evaporation-condensation [29,31]. In the temperature and bubble size regime of interest to the present problem the surface diffusion mechanism should be most relevant. For surface diffusion controlled bubble migration the diffusivity is expressed as [29,31]:

$$D_b = \frac{3D_S\omega^{4/3}}{4\pi R_b^4},$$

where $D_s$ is the surface diffusion coefficient, $R_b$ the bubble radius and $\omega$ is the atomic volume of uranium ions. We have calculated the activation energy for surface diffusion on the $UO_2$ (111) surface to be 1.26 eV, which is close to the activation energy reported by Turnbull (1.2 eV) [11], by combining the segregation energy, the migration barrier for uranium divacancies in the near surface region and the bulk concentration of uranium vacancies and divacancies obtained from MARMOT simulations [2,3]. The (111) surface is the most stable in $UO_2$ and it is here assumed to form the bounding surface of small fission gas bubbles. As for bulk diffusion the migration barrier of single uranium vacancies is higher and gives much lower diffusion rates than for divacancies. The pre-exponential factor is given by the attempt frequency, the segregation entropy, the pre-exponential for the bulk divacancy concentration and the bubble radius. The attempt frequency for surface diffusion of divacancies is about $2.7\times10^{11}$ $s^{-1}$ and the pre-exponential factor for the bulk concentration of divacancies is known from MARMOT simulations. We have attempted to calculate the segregation entropy, but are still encountering challenges. Our current results indicate negative segregation entropies (vibrational), which would not be consistent with the bubble diffusion mechanism (the pre-exponential factor would be too low for all fission gas bubble radii) and it is also somewhat counterintuitive. The radius of bubbles cannot yet be determined from our simulations, but are typically assumed to be up to a few nanometers. Until these two (partially) unknown parameters are determined, we cannot make an accurate prediction of the bubble diffusion coefficient.

Regardless, we have plotted the bubble diffusivity arising from the present model in Figure 9. However, to circumvent the unknowns mentioned above, the pre-

exponential factor was chosen to match the experimental model, which, despite the corresponding parameter values being reasonable, implies that the model is not a first principles prediction. If the segregation entropy is assumed to be ~7$k_B$, the experimental irradiation-enhanced diffusivity is reproduced for bubbles of radius ~1 nm. Both the assumed segregation entropy and the resulting size of bubbles are unreasonable. Even though the agreement with the experimental data is encouraging, bubble diffusion mechanisms must be further investigated before solid conclusions can be drawn. In addition to the uncertainty or difficulties estimating surface segregation entropies, the surface diffusion rate calculated above may not translate to small clusters exhibiting deviations from perfect (111) surfaces. The imperfections can act as trap states significantly reducing the diffusion rates. It is also possible that the Xe atoms inside the bubble block migration of surface uranium ions thus impeding vacancy and bubble migration. Finally, bubble diffusion would also require some internal re-arrangement of the bubble, in addition to vacancy diffusion, and it is not easy to know a priori what the corresponding rate would be. These mechanisms lowering the bubble diffusivity would be consistent with the lack of experimental confirmation of high bubble mobility, at least for easily observable bubbles under out-of-pile conditions. Nevertheless, the low migration barrier of surface vacancies and the reasonable agreement obtained for the activation energy of bubble diffusion as well as the pre-exponential factor under certain assumptions (see above) motivate explicit investigation of small fission gas bubbles. This is necessary to confirm the above hypothesis of bubble or extended cluster migration being responsible for irradiation-enhanced Xe diffusion at intermediate to low temperatures.

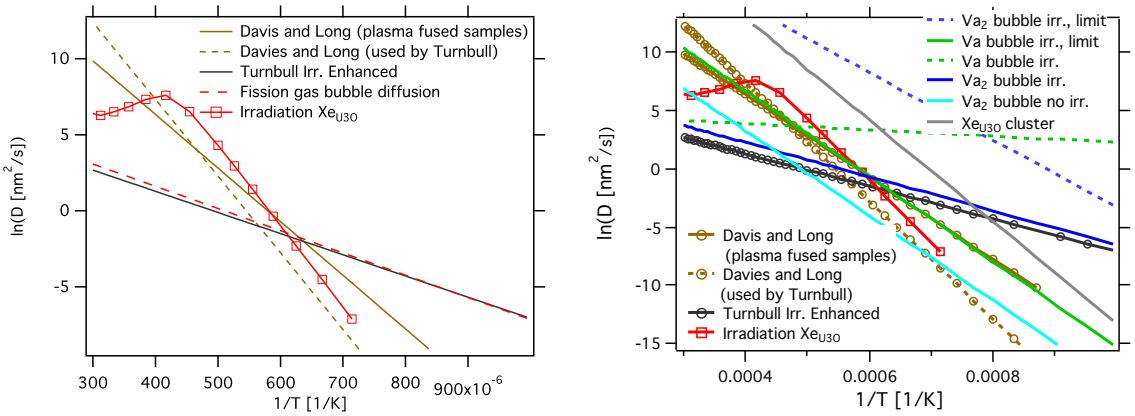


**Figure 9: Left) The effective Xe diffusion coefficient under irradiation conditions including the $Xe_{U3O}$ cluster compared to the experimental model proposed by Turnbull [11,12]. We also include the diffusivity for fission gas bubbles with surface diffusion as the rate-limiting step and the pre-exponential factor fitted to Turnbull's data [11,12], which is also consistent with diffusion models (see text). Right) This plot shows similar data as the left hand figure, but includes detailed results for bubble diffusion mechanisms with the segregation entropies assumed to be 7.19$k_B$ and 5.82$k_B$ for divacancies and vacancies, respectively.**

## 3.4 Diffusion of octahedron uranium vacancy clusters containing Xe atoms

We have already studied the $Xe_{U2O}$ (Xe in a uranium plus oxygen vacancy trap site with another uranium vacancy providing the pathway for diffusion) and $Xe_{U3O}$ (Xe in a uranium plus oxygen vacancy trap site with two other uranium vacancies providing the pathway for diffusion) clusters. In order to investigate how even larger Xe-vacancy clusters contribute to diffusion we have calculated vacancy binding energies and migration barriers for clusters containing four ($Xe_{U4Ox}$), five ($Xe_{U5Ox}$) and six ($Xe_{U6Ox}$) uranium vacancies. Different number and configurations of oxygen vacancies were tried for each cluster. All clusters are presently assumed to be neutral, which implies that the difference in charge between the uranium and oxygen vacancies is compensated by $U^{5+}$ ions. Future calculations will consider partially charged Xe clusters, similar to what was already done for the smaller $Xe_{U2O}$ and $Xe_{U3O}$ clusters. Some of the extended clusters are illustrated in Figure 10. This investigation was exploratory and we have not performed a complete search over the full configuration space, but at the same time we have covered enough configurations to determine the general diffusion behavior. The effective migration barriers for clusters composed of three, four, five and six vacancies bound to the original single vacancy Xe trap site are similar to the cluster with two bound vacancies, close to 4 eV, or higher. These clusters consequently diffuse with a rate similar to the $Xe_{U3O}$ cluster, which is too slow to explain the low temperature radiation-enhanced diffusivity observed in experiments but it is consistent with the diffusion properties observed in the intrinsic regime. The binding energies of uranium vacancies to these clusters vary based on the number oxygen vacancies and charge state of the cluster.

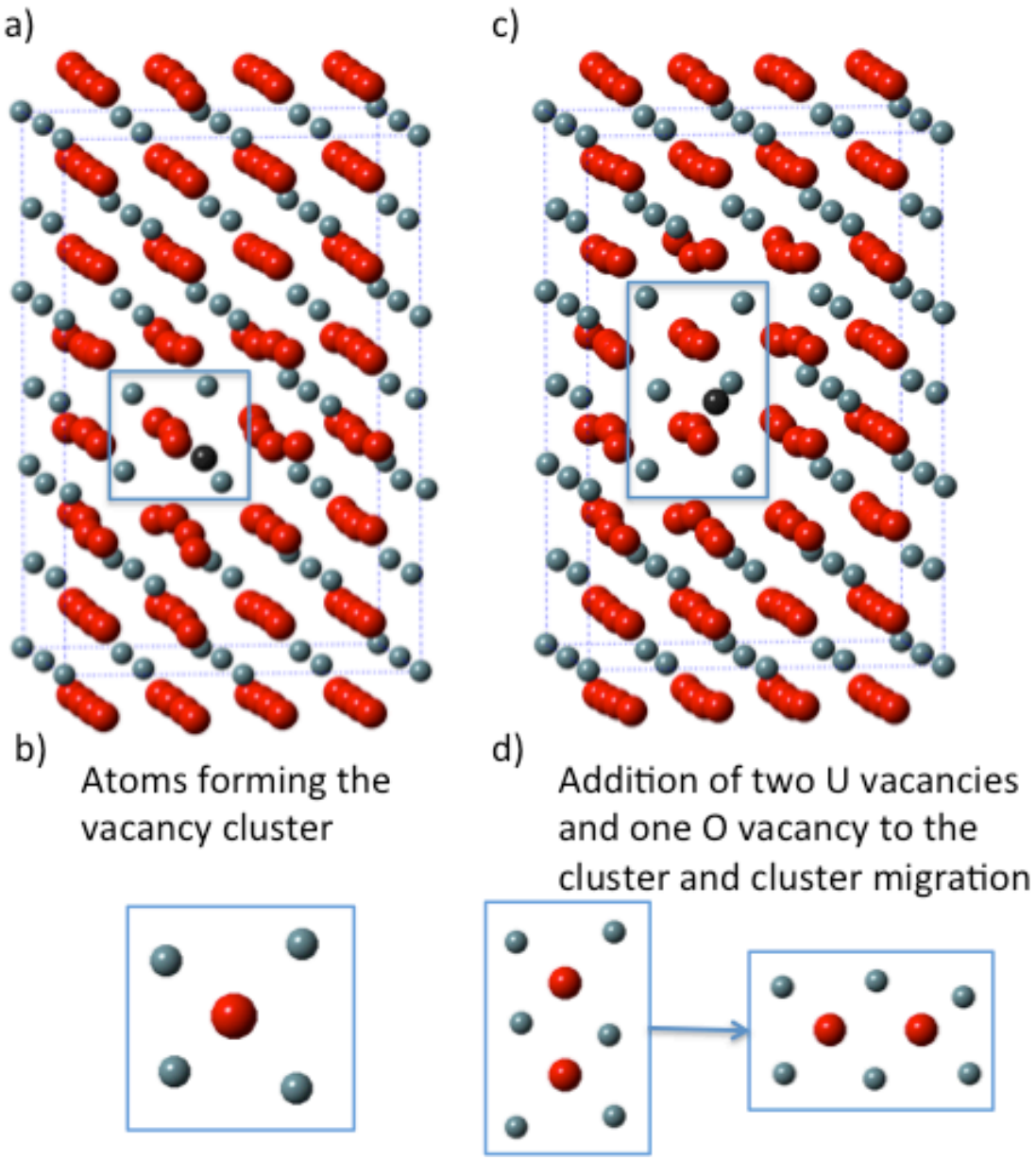


**Figure 10: a) The $Xe_{U4O}$ (four uranium vacancies and one oxygen vacancy) cluster is highlighted in the box. b) Representation of the ions constituting the $Xe_{U4O}$ cluster. The Xe atom is not shown. c) The diffusion mechanism for the $Xe_{U4O}$ cluster was investigated for both single uranium vacancies and divacancies. Here, the cluster and mechanism involving two vacancies is illustrated and highlighted in the box. d) The vacancies constituting the $Xe_{U4O}$ cluster plus the two additional vacancies enabling diffusion are shown. The Xe atom is not shown. The second figure illustrates the vacancy configuration after completing a migration step. The corresponding barriers are too high to explain the irradiation-enhanced Xe diffusion observed in experiments. In all figures, uranium ions or vacancies are shown in grey and oxygen ions or vacancies in red.**

The cluster containing six uranium vacancies in Figure 10 can be transformed into a much more stable arrangement by adding more oxygen vacancies and reconfiguring into an octahedron ($Xe_{U6O8}$), see Figure 11. This is intuitively obvious when inspecting its compact structure. Essentially, this represents a small (the smallest) bubble bounded by (111) surfaces, which are known to be the most stable in $UO_2$.

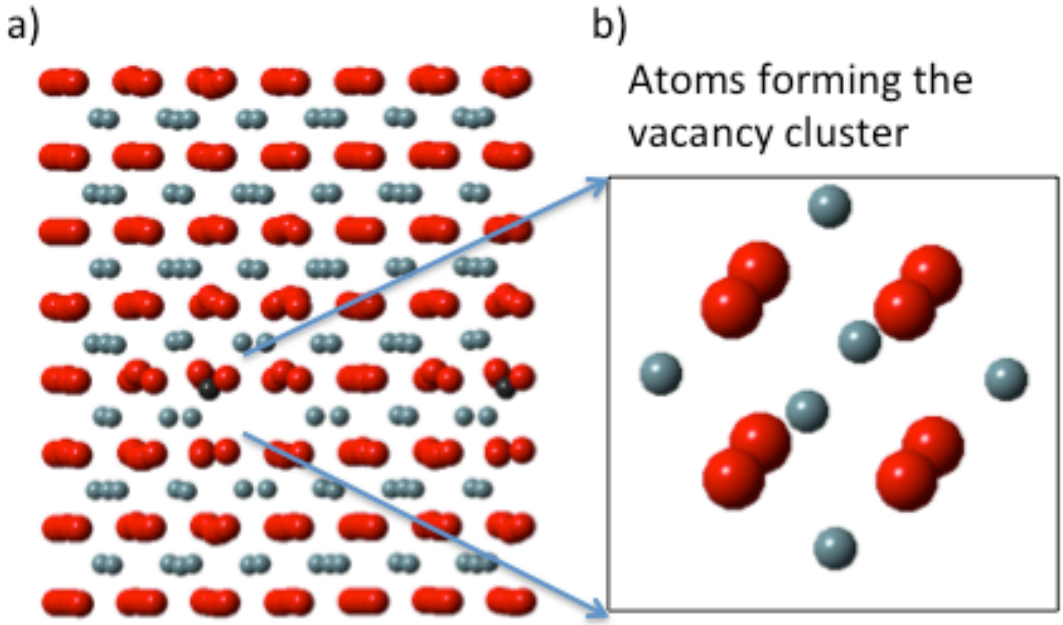


**Figure 11: a) The most stable Xe-vacancy cluster containing six uranium ions forming an octahedron and eight oxygen vacancies as well as a Xe atom ($Xe_{U6O8}$). b) The vacancies constituting the $Xe_{U6O8}$ cluster are highlighted. The Xe atom is not shown. Uranium ions or vacancies are shown in grey and oxygen ions or vacancies in red.**

We have investigated binding of single uranium vacancies to this cluster and then migration of this vacancy around the cluster, which is a necessary step for long-range fission gas diffusion. The single vacancies exhibit rather high migration barriers, generally 4 eV or higher, which is consistent with bulk diffusion of uranium vacancies. These barriers are again too high to explain the radiation-enhanced diffusion rates observed in experiments. Moreover, we have not been able to identify a favorable mechanism for single uranium vacancies that leads to translation of the cluster, i.e. the migration steps referenced above only involve migration around the cluster and its center of mass is unchanged.

However, as for bulk diffusion, the migration barrier decreases to about 2-3 eV (see Table 2 and Figure 12) for uranium divacancies migrating around the $Xe_{U6O8}$ cluster, and there is also a mechanism that enables rapid translation of the cluster center of mass. The $Xe_{U6O8}$ cluster with two additional uranium vacancies is denoted $Xe_{U8O8}$. The migration steps are illustrated in Figure 12 and taken together they give rise to fast fission gas diffusion. The barriers are still being evaluated and the numbers listed in Table 2 and Figure 12 should be treated as preliminary or rather upper bounds. There are several options for the migration steps around the cluster. Figure 12 illustrates one set of steps leading to a complete migration step. The lowest barriers are obtained by decreasing the number of nearest neighbor uranium ions at the saddle point, which is close to the octahedral interstitial site. Note that both the steps around and across the cluster are necessary to give rise to long-range diffusion. The translation step occurs by one of the uranium vacancies moving

towards the bound uranium divacancy, see Figure 12. This step is facilitated by first rearranging the oxygen vacancies in order to prevent the migrating uranium ion from being under coordinated. The barrier for this step is about 2 eV. The migration barriers for oxygen ions are very low compared to the barriers for uranium ions. Consequently, the oxygen migration steps should not impact the cluster diffusion rate significantly. The same conclusion holds for rearranging the Xe atoms within the cluster. The second symmetrically equivalent uranium ion can move according to the same mechanism after the oxygen ions have been rearranged to complete the translation step.

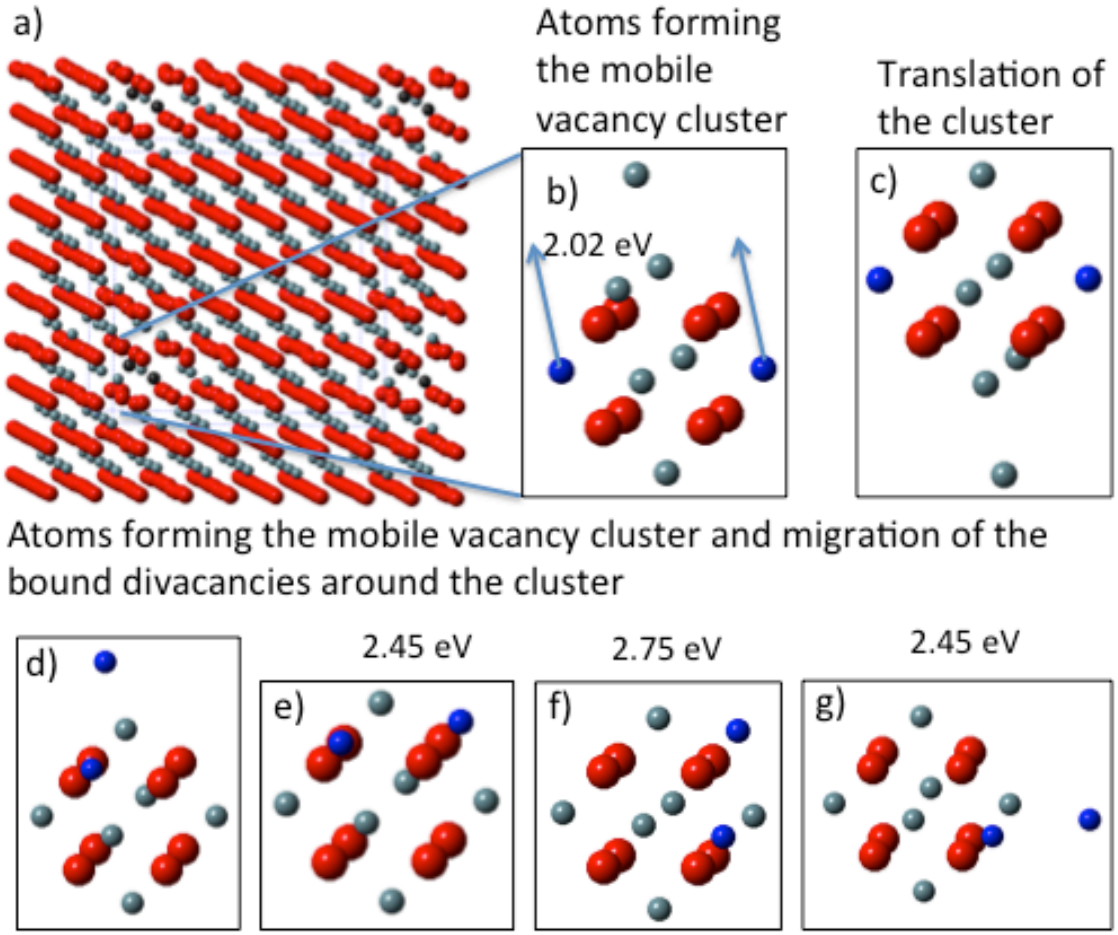


**Figure 12: a) The $Xe_{U6O8}$ diffusion mechanism involving two bound uranium vacancies. b) and c) illustrate the translation step. The two migrating vacancies (symmetrically equivalent) are highlighted in blue. They migrate separately and the motion is facilitated by rearranging the oxygen vacancies. The final cluster is equivalent to the starting cluster but the center of mass and thus the Xe atom has been translated. d), e), f) and g) show the two uranium vacancies (highlighted in blue) moving around the Xe cluster to recover a cluster that is symmetrically equivalent the initial cluster. Combined with the translation motion (b) and c)), this leads to net migration of the cluster.**

Just as for the small clusters, the diffusion coefficient for the $Xe_{U6O8}$ cluster involves the migration properties (described above) and the concentration of mobile clusters or the fraction of the $Xe_{U6O8}$ clusters that have bound divacancies. The latter is governed by the binding energy and the concentration of vacancies and divacancies in the bulk. The binding energy is close to zero, see Table 2, and the concentration in

the bulk is governed by the irradiation conditions as previously calculated by MARMOT simulations [2]. Unlike the smaller clusters ($Xe_{U2O}$ and $Xe_{U3O}$), the vacancies are not as strongly bound to the larger $Xe_{U6O8}$ cluster. Combining the migration barrier, binding energy and the concentration of divacancies (at intermediate to low temperature) we obtain activation energy of 1.7 eV for bubble diffusion, which is of the same order of magnitude as the experimentally observed value. The attempt frequency was calculated to be approximately $6.4\times10^{11}$ $s^{-1}$. However, the segregation entropy and the correlation factor for the multi-step mechanism involved in $Xe_{U6O8}$ diffusion remain to be determined. Until that is completed the pre-exponential factor is unknown. Nevertheless, the pre-exponential factor should be similar to that estimated for fission gas bubbles in the previous section, which showed favorable agreement with experiments under certain assumptions.

We are continuing to work on the details of the extended cluster diffusion mechanisms. These mechanisms will also be implemented in the MARMOT fission gas diffusion model in order to couple the bubble behavior to other defect fluxes.

**Table 2: The binding energy of vacancies to the octahedron $Xe_{U6O8}$ cluster and migration properties of the resulting $Xe_{U8O8}$ cluster. The migration steps are illsutrated in Figure 12.**

| | Binding of two vacancies to $Xe_{U6O8}$ -> $Xe_{U8O8}$ | Migration of $Xe_{U8O8}$, translation | Migration of $Xe_{U8O8}$, rotation step 1 | Migration of $Xe_{U8O8}$, step 2 | Migration of $Xe_{U8O8}$, step 3 |
|---|---|---|---|---|---|
| Energy (eV) | -0.02 | 2.02 | 2.20 | 2.75 | 2.20 |

# 4. Conclusions

The fission gas diffusion coefficient is one of the key parameters controlling fission gas retention and release. This report has summarized progress in understanding and modeling fission gas (Xe and Kr) and fission product (Zr, Ru, Ce, Y, La, Sr and Ba) diffusion in uranium dioxide fuel. We have studied diffusion under both intrinsic and in-pile conditions using density functional theory calculations, empirical potential calculations and MARMOT simulations. The results have also been coupled to BISON engineering scale simulations of fission gas release and compared to a few test cases. Comparison to experimental data indicates that our simulations underestimate the diffusivity across a large temperature range including both intrinsic and irradiation-enhanced diffusion. The same conclusion holds true for self-diffusion of uranium.

The present study has addressed this issue by investigating diffusion of extended (large) Xe-vacancy diffusion or small fission gas bubbles as well as uranium divacancies. This contrasts the traditional assumption, used in empirical Xe diffusion models and also adopted by us in earlier studies, that Xe atoms migrate by

a vacancy mechanisms involving Xe atoms occupying a uranium vacancy (possibly with additional oxygen vacancies) trap site and a single additional vacancy providing the pathway for diffusion. First, we studied a cluster involving Xe in a uranium vacancy trap site and two additional uranium vacancies ($Xe_{U3O}$), instead of one vacancy ($Xe_{U2O}$) as previously assumed. This cluster is quite stable and has a lower migration barrier than the single vacancy trap site cluster by approximately 1 eV. Even though this cluster only exists in small concentrations, its high mobility leads to increased diffusivity for an extended temperature range, which gives much better agreement with available experimental data. Interestingly, the $Xe_{U3O}$ cluster gives rise to effective Xe diffusivities that are higher for intrinsic conditions than under irradiation for a wide range of temperatures. Under irradiation the fast-moving $Xe_{U3O}$ cluster recombines quickly with irradiation induced interstitial U ions, while this mechanism is much less important for intrinsic conditions. The net result is higher concentration of the $Xe_{U3O}$ cluster for intrinsic conditions than under irradiation. This behavior finds support in experiments and can explain the surprisingly wide range of diffusivities reported in different experimental studies.

However, all the vacancy-mediated mechanisms investigated so far underestimate the Xe diffusivity compared to the irradiation-enhanced diffusion coefficient observed in experiments. It is important to understand this discrepancy, since nuclear fuel typically operates at temperatures where irradiation-enhanced diffusion dominates over intrinsic diffusion. The hypothesis that we have been working from is that extended Xe-vacancy clusters may diffuse fast by mimicking the mechanism that gives rise to a low migration barrier for uranium divacancies compared to single vacancies. Diffusion of extended clusters or small bubbles is also consistent with the low pre-exponential factor observed in the irradiation-enhanced regime. We have used DFT calculations to investigate binding of vacancies to small fission gas bubbles, which were modeled as simplified (111) surfaces and as explicit octahedron clusters of six uranium vacancies and additional eight oxygen vacancies. Both models predict low migration barriers consistent with experiments. Compared to the smaller clusters ($Xe_{U2O}$ and $Xe_{U3O}$) the vacancy binding energies are lower (less attractive). Taken together these properties are consistent with experimental observations, however additional work is still required before we can solidify our conclusions. The octahedron cluster shows intriguing diffusion properties combined with high stability. It migrates by a multi-step mechanism involving coupled motion of uranium and oxygen vacancies. We will continue to study the properties of the octahedron cluster and also expand current MARMOT models to include the larger clusters and couple them to other defect fluxes.

# 5. References


[1] D. A. Andersson, B. P. Uberuaga, P. V. Nerikar, C. Unal, C. R. Stanek, Phys. Rev. B **84**, 054105 (2011).

[2] D. A. Andersson, P. Garcia, X.-Y. Liu, G. Pastore, M. Tonks, P. Millett, B. Dorado, D. R. Gaston, D. Andrs, R. L. Williamson, R. C. Martineau, B. P. Uberuaga, C. R. Stanek, J. Nucl. Mater. **451**, 225 (2014).

[3] D. A. Andersson, M. R. Tonks, L. Casillas, S. Vyas, P. Nerikar, B. P. Uberuaga, C. R. Stanek, J. Nucl. Mater. **462**, 15 (2015).

[4] X.-Y. Liu and D. A. Andersson, J. Nucl. Mater. **462**, 8 (2015).

[5] X.-Y. Liu, B. P. Uberuaga, D. A. Andersson, C. R. Stanek, K. E. Sickafus, Appl. Phys. Lett. **98**, 151902 (2011).

[6] E. Vathonne, D. A. Andersson, M. Freyss, C. R. Stanek and M. Bertolus, "Electronic structure investigation of krypton atomic migration in uranium dioxide", to be published.

[7]. P. V. Nerikar, D. C. Parfitt, L. A. Casillas Trujillo, D. A. Andersson, C. Unal, S. B. Sinnott, R. W. Grimes, B. P. Uberuaga, C. R. Stanek, Phys. Rev. B **84**, 174105 (2011).

[8] R. Perriot, X.-Y. Liu, C. R. Stanek, D. A. Andersson, J. Nucl. Mater. **459**, 90 (2015).

[9] J. A. Turnbull, J. Nucl. Mater. **50**, 62 (1974).

[10] J. A. Turnbull, C. A. Friskney, J. Nucl. Mater. **71**, 238 (1978).

[11] J. A. Turnbull, C. A. Friskney, J. R. Findlay, F. A. Johnson, A. J. Walter, J. Nucl. Mater. **107**, 168 (1982).

[12] J. A. Turnbull, R. J. White, C. Wise, in: Proceedings of Technical Committee Meeting on Water Reactor Fuel Element Computer Modelling in Steady State, Transient and Accident Conditions, Preston, UK, Sept. 18-22, pp. 174.

[13] D. Davies, G. Long, The emission of xenon-133 from lightly irradiated uranium dioxide spheroids and powders, Technical Report AERE Rep. No. 4347, Atomic Energy Research Establishment, Harwell, 1963.

[14] W. Miekeley, F. W. Felix, J. Nucl. Mater. **42**, 297 (1972).

[15] H. J. Matzke, Radiat. Eff. Defect S. **83**, 219 (1980).

[16] R. J. White, M. O. Tucker, J. Nucl. Mater. **118**, 1 (1983).

[17] G. T. Lawrence, J. Nucl. Mater. **71**, 195 (1978).

[18] R. M. Cornell, Phil. Mag. **19**, 539 (1969).

[19] K. N. G. Kaimal, M. C. Naik, A. R. Paul, J. Nucl. Mater. **168**, 188 (1989).

[20] H. J. Matzke, J. Chem. Soc. Faraday Trans. 2 **83**, 1121 (1987).

[21] The Third Risö Fission Gas Project, BUMP TEST AN3 (CB8-2R), Technical Report RISÖ-FGP3-AN3, 1990.

[22] Fuel Modelling at Extended Burnup (FUMEX-II), Technical Report Technical Report IAEA-TECDOC-1687, IAEA, IAEA, 2012.

[23] B. Basak, A.K. Sengupta, H.S. Kamath, J. Alloys Compd. **360**, 210 (2003).

[24] S. Lany, A. Zunger, Phys. Rev. B **78**, 235104 (2008).

[25] M. Tonks, D. Gaston, P. Millett, D. Andrs, P. Talbot, Compos. Mater. Sci. **51**, 20 (2012).

[26] A. Goyal, S. R. Phillpot, G. Subramanian, D. A. Andersson, Chris R. Stanek, Blas P. Uberuaga, Phys. Rev. B **91**, 094103 (2015).

[27] B. Dorado, D. A. Andersson, C. R. Stanek, M. Bertolus, B. P. Uberuaga, G. Martin, M. Freyss, P. Garcia, Phys. Rev. B **86**, 035110 (2012).
[28] J. R. MacEwan, W. H. Stevens, J. Nucl. Mater. **11**, 77 (1964).
[29] J. A. Turnbull, J. Nucl. Mater. **62**, 325 (1976).
[30] C. Baker, J. Nucl. Mater. **66**, 283 (1977).
[31] M. S. Veshchunov, V. E. Shestak, J. Nucl. Mater. **376**, 174 (2008).